

Quantitative determination of optical trapping strength and viscoelastic moduli inside living cells

This article has been downloaded from IOPscience. Please scroll down to see the full text article.

2013 Phys. Biol. 10 046006

(<http://iopscience.iop.org/1478-3975/10/4/046006>)

View [the table of contents for this issue](#), or go to the [journal homepage](#) for more

Download details:

IP Address: 130.225.212.4

The article was downloaded on 26/08/2013 at 10:02

Please note that [terms and conditions apply](#).

Quantitative determination of optical trapping strength and viscoelastic moduli inside living cells

Josep Mas^{1,2,3}, Andrew C Richardson², S Nader S Reihani^{2,4},
Lene B Oddershede² and Kirstine Berg-Sørensen¹

¹ Department of Physics, Technical University of Denmark, Kgs Lyngby, Denmark

² The Niels Bohr Institute, University of Copenhagen, Copenhagen, Denmark

³ Optical Trapping Lab, Department of Optics and Applied Physics, Barcelona, Spain

⁴ Department of Physics, Sharif University of Technology, Tehran 11365-9161, Iran

E-mail: kirstine.berg-sorensen@fysik.dtu.dk

Received 19 November 2012

Accepted for publication 7 June 2013

Published 2 July 2013

Online at stacks.iop.org/PhysBio/10/046006

Abstract

With the success of *in vitro* single-molecule force measurements obtained in recent years, the next step is to perform quantitative force measurements inside a living cell. Optical traps have proven excellent tools for manipulation, also *in vivo*, where they can be essentially non-invasive under correct wavelength and exposure conditions. It is a pre-requisite for *in vivo* quantitative force measurements that a precise and reliable force calibration of the tweezers is performed. There are well-established calibration protocols in purely viscous environments; however, as the cellular cytoplasm is viscoelastic, it would be incorrect to use a calibration procedure relying on a viscous environment. Here we demonstrate a method to perform a correct force calibration inside a living cell. This method (theoretically proposed in Fischer and Berg-Sørensen (2007 *J. Opt. A: Pure Appl. Opt.* **9** S239)) takes into account the viscoelastic properties of the cytoplasm and relies on a combination of active and passive recordings of the motion of the cytoplasmic object of interest. The calibration procedure allows us to extract absolute values for the viscoelastic moduli of the living cell cytoplasm as well as the force constant describing the optical trap, thus paving the way for quantitative force measurements inside the living cell. Here, we determine both the spring constant of the optical trap and the elastic contribution from the cytoplasm, influencing the motion of naturally occurring tracer particles. The viscoelastic moduli that we find are of the same order of magnitude as moduli found in other cell types by alternative methods.

 Online supplementary data available from stacks.iop.org/PhysBio/10/046006/mmedia

1. Introduction

Over the past decade, high-quality quantitative measurements of the forces exerted by or acted upon individual bio-molecules have emerged [1–4]. The vast majority of reported quantitative force measurements were performed *in vitro*. While *in vitro* studies have many qualities, for instance that individual action–reaction mechanisms can be isolated, the natural next step is to move *in vivo* and quantitatively investigate which forces are acting inside a living organism where the molecular

motors' function in their native environment. However, as the cytoplasm is a dynamic and very complex environment, this is a challenging task [5, 6].

Optical tweezers have proven an excellent tool for *in vitro* measurements of forces at the single-molecule level, and reliable and precise calibration techniques exist which provide the platform necessary to perform a quantitative force measurement in a purely viscous environment [7–9]. As biological tissue is only weakly absorbing in the near-infrared

regime, optical tweezers based on infrared lasers have been shown to be nearly non-invasive if the total amount of deposited energy is kept low [10, 11]. This also implies that heating is rarely a problem [12]. Other techniques also function well for *in vivo* measurements, for instance atomic force microscopy and magnetic tweezers. In contrast to the former which cannot reach inside the cell without penetrating the cell wall and the latter which requires a magnetic internalized handle, optical tweezers have the benefits that they can reach inside the cell without disrupting the cell wall and it can trap cellular organelles, e.g., lipid granules, without the need for chemical modifications or internalization of foreign handles [6].

If microrheological measurements are made, information about, e.g., the diffusion of tracers [13–15] or the viscoelastic moduli of the cytoplasm [16, 17] or a reconstituted polymer network [18, 19] can be returned without the knowledge of, e.g., the absolute spring constant characterizing the harmonic potential of the optical trap. This value, however, would be needed in order to perform a quantitative force measurement inside the cell in further applications of the method, for instance, to measure the forces acting on the cytoskeleton during cell division, the force exerted by a molecular motor or the force exerted by a polymerizing microtubule.

It is widely known that the trap spring constant depends on several system parameters such as the trapping beam power, wavelength, numerical aperture and optical aberrations, together with local properties of the sample like the trapped particle size, and the medium and particle refractive indexes [20]. Hence the spring constant must be calibrated for each trapped object in order to convert position measurements to force measurements. Even though several standard approaches exist for calibrating the force of the trap in viscous media [21], the lack of a specific method for calibrating the trap force in complex environments like the inner cell makes intracellular force measurements a challenge.

One possible way to tackle this problem is to perform trap force calibrations with purified organelles in a viscous buffer, where standard methods apply. If the refractive index of the buffer is properly tuned to mimic the cell cytoplasm, one can in principle extrapolate the calibrated stiffness to apply it in experiments taking place inside the cell. In this case, one must account for phenomenological correlations between trap stiffness and microscopy image contrast [22] or particle size [23]. This sophisticated way for quantifying the trap spring constant circumvents the lack of a proper method for calibrating the trap force in living cells, although an *in situ* calibration would be preferred for taking into account all the local conditions *in vivo*. For example, *ex situ* calibrations do not consider elements in the cell, like membranous structures in the path of the laser, that might introduce local optical aberrations affecting the actual trap stiffness. Also, local variations in the cell refractive index around the trap due to the presence of cellular structures would introduce changes in the trapping strength with respect to the viscous buffer. Very recent work suggests to calibrate within the cell based on an assumed model with five corresponding fitting parameters of the viscoelastic response of the intercellular medium. This method has been demonstrated for phagocytosed latex beads of known size [24].

An alternative method applicable in a living cell is based on the detection of light momentum changes [25], which requires the ability to detect momenta of the major part of the photons interacting with the sample to infer the net force exerted by the laser beam. Although this is technically challenging, it has recently been compatibilized with single-beam optical traps [26, 27] and applied to *in vivo* molecular motor force measurements in living *Allium cepa* cells [28]. This method is sample independent and directly supplies the net optical force acting on any trapped object, which could be used as a handle for studying the biological forces acting thereon. However, the method does not provide information on local parameters that also have interest *per se* like the trap spring constant (e.g., for studying the optical trap strength dependence on the trapped intracellular organelle), particle position (e.g., for diffusion studies) or viscoelastic properties of the cell cytoplasm. Moreover, care must be taken when applying this method in order to avoid uncontrolled optical scatterers in the path of the laser (e.g., turbid samples, tissues or membranous structures) that could significantly mask the measurement of the force acting on the trapped object.

Here, we demonstrate how to perform *in situ* force calibration of optical tweezers in the cytoplasm of a living cell, with no need of external calibrations or additional assumptions about the viscoelastic medium. Our method takes into account the viscoelastic nature of the cell cytoplasm and returns the absolute value of the spring constant for each trapped organelle in the cell cytoplasm, as shown in section 4. One very significant advantage of our method is that trap calibration does not require the knowledge of the size nor shape of the force-transducing handle. The method combines passive measurements where the diffusion of the tracer is monitored with active measurement in which the confining potential is oscillated, while the response of the tracer is monitored. This type of combined active and passive measurement was previously proposed as a valid way to calibrate in viscoelastic media [29–32] and here demonstrated inside a living *S. pombe* cell, thus paving the way for quantitative *in vivo* force measurements at the single-molecule level for biological forces acting on optically trapped organelles. Very recently, the active–passive calibration method with laser driving rather than stage driving has been applied in investigations of molecular motor proteins in A549 human epithelial cells and in *Dictyostelium discoideum* [33]. In this work, in addition to trap characteristics, quantitative material characteristics in the form of viscoelastic moduli of the cytoplasm are extracted.

2. Active–passive calibration

The optical trap is assumed to exert a harmonic force, F , on the trapped object. Hence, $F = \kappa x$, where κ is the spring constant characterizing the optical trap and x is the deviation of the trapped object from its equilibrium position. We wish to extract an absolute number for κ inside a living cell, which together with a measurement of x will allow for a quantification of the applied force, F . Also, we wish to extract the viscoelastic moduli characterizing the living cell cytoplasm. To this end, the results from active and passive calibration measurements are

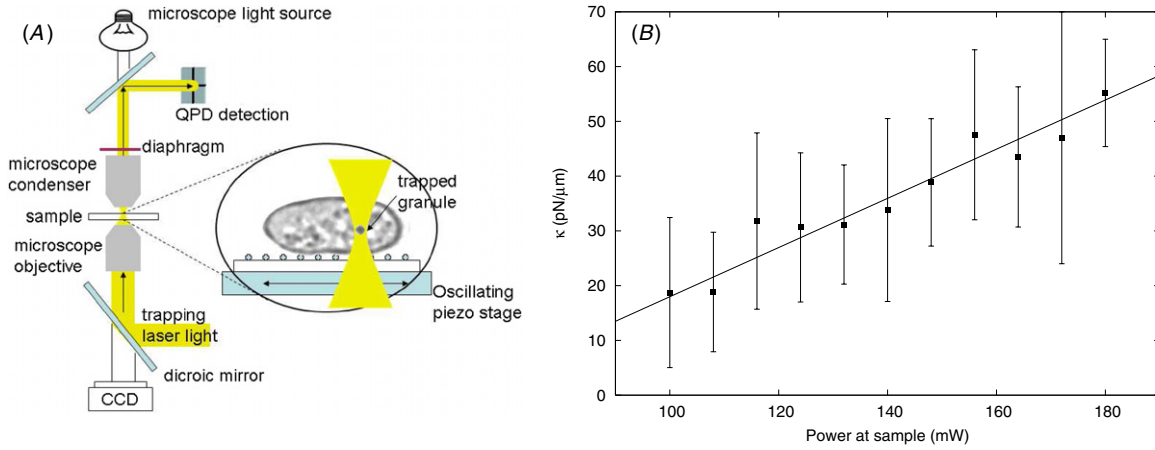


Figure 1. (A) Sketch of the experimental setup. A living *S. pombe* yeast cell is immobilized on a coverslip. An endogenously occurring lipid granule is optically trapped. The position of the granule is recorded both by a quadrant photodiode (QPD) and by a CCD camera. In the passive experiments, the granule performs a thermally induced stochastic motion, in the active experiments, the sample is oscillated in a controlled fashion by a piezo-stage. (B) The spring constant of the optical trap measured repeatedly on the same cytoplasmic granule for increasing laser power. As expected, κ increases linearly with power.

combined. In the active measurements, the sample is moved in an oscillatory fashion with respect to the confining laser trap, and in the passive measurements, the thermal diffusion of a tracer is simply monitored. The experimental setup is sketched in figure 1(A).

The idea of combining active and passive measurements for quantitative *in vivo* measurements has been put forward in [29–31, 19] and suggested to be part of a custom calibration procedure of an optical trap [34]. The underlying principle is that of linear response theory, which connects a response function of the medium, $\chi(\omega)$, to the average Fourier-transformed $\langle \tilde{x}(\omega) \rangle$ of an observed position x of a tracer particle, and the Fourier-transformed \tilde{F}_{ext} of an external force F_{ext} ,

$$\langle \tilde{x}(\omega) \rangle = \chi(\omega) \tilde{F}_{\text{ext}}(\omega). \quad (1)$$

The exact formulas used in this work were derived in [31] and tested in an actin network [32], and we refer the interested reader to these two papers for more details on the theoretical framework. Here, we only present the equations necessary for data analysis.

Passive measurements. In series of passive measurements, timeseries of the positions visited by an optically trapped object, $x_p(t_i)$, were recorded for $t_i \in [0, T_{\text{meas}}]$, where t_i is the i th measurement of time and T_{meas} is the total measurement time. From these timeseries, the power spectrum $P(\omega)$ of the positional fluctuations in the trap was calculated as

$$P(\omega) = \lim_{T_{\text{meas}} \rightarrow \infty} \frac{\langle |\tilde{x}_p(\omega)|^2 \rangle}{T_{\text{meas}}}, \quad (2)$$

where $\tilde{x}_p(\omega)$ is the Fourier transformed of the position of the trapped particle and $\omega = 2\pi f$ is the angular frequency (f is the normal frequency).

Active measurements. In the experiments discussed here, the trapped object (an endogenous granule) was oscillated in a sinusoidal fashion by oscillating the entire stage. Hence, the position of the stage can be described by $x_s(t) = A_s \sin \omega t$, where A_s is the amplitude of the stage motion. Simultaneously,

the position of the driven trapped object, $x_p^{(\text{dr})}(t)$, was recorded. The amplitude A_s of the stage position, x_s , and the driving frequency, ω , were chosen within limits set by the underlying assumptions, assuring that the response remains linear [31].

The relaxation spectrum, $\tilde{R}(\omega)$, defined as

$$\tilde{R}(\omega) = \frac{\langle \tilde{x}_p^{(\text{dr})}(\omega) \rangle}{i\omega \tilde{x}_s(\omega)} \quad (3)$$

may be extracted either directly from equation (3) or, more conveniently, via the phase-difference $\Delta\phi$ between the phase of the induced stage driving, ϕ_s , and the phase of the resulting oscillatory motion of the trapped object, ϕ_p ,

$$\Delta\phi = \phi_p - \phi_s, \quad (4)$$

$$\tilde{R}(\omega) = \frac{A_p}{\omega A_s} (\sin \Delta\phi - i \cos \Delta\phi). \quad (5)$$

As the amplitude of the stage driving, A_s , is known, $\Delta\phi$ and the amplitude of the sinusoidal motion of the particle, A_p , can be extracted from fits of equation (5) to the experimental data.

Extracting characteristics of the optical trap and of the viscoelastic medium. From the quantities defined above and obtained through passive and active measurements, the spring constant characterizing the optical trap, κ , can be found:

$$\kappa - \omega^2 m = 2k_B T \frac{\text{Re}(\tilde{R}(\omega))}{P(\omega)}. \quad (6)$$

From this value, the viscoelastic modulus, $G(\omega)$, characterizing the viscoelastic cytoplasm can be extracted:

$$G(\omega) = \frac{i\omega}{6\pi r} (\kappa - \omega^2 m) \frac{\tilde{R}(\omega)}{1 - i\omega \tilde{R}(\omega)}. \quad (7)$$

If the stage is driven sinusoidally at frequency ω_s , equation (6) becomes

$$\kappa - \omega_s^2 m = \frac{2k_B T}{P(\omega_s)} \frac{A_p}{\omega_s A_s} \sin(\Delta\phi). \quad (8)$$

In equations (6)–(8), m denotes the mass of the trapped object and r its radius. We note that in order to determine κ ,

the knowledge of the size r of the trapped object is not needed. Also, often and in particular in the experiments presented below, the frequency is so small that terms including $\omega^2 m$ are significantly smaller than any of the other terms in those equations. Hence, they can be safely neglected and it is not necessary to estimate m .

For completeness, we also note that the response function of the medium, $\chi(\omega)$, cf equation (1), may be found as

$$\chi(\omega) = \frac{1 - i\omega\tilde{R}(\omega)}{\kappa - \omega^2 m} \simeq \frac{1 - i\omega\tilde{R}(\omega)}{\kappa}, \quad (9)$$

and we may extract an effective spring constant, e.g., the combined spring constant for all elastic forces felt by the trapped object

$$\kappa_{\text{eff}} = \frac{1}{|\chi(\omega)|}. \quad (10)$$

This effective spring constant contains contributions from both optical trap and viscoelastic medium.

3. Materials and methods

3.1. Preparation of biological samples

The *S. pombe* cells (SPK10, wildtype) were cultured on agar plates (AA minus leucine) at 30 °C for 18–20 h and then stored at 4 °C. A small amount of the cells were transferred from the agar plate to a rich liquid YPD medium (Sigma Y1375) and grown overnight at 30 °C in a shaking water bath. Cells were harvested by centrifuging for 5 min at 5000 rpm. The cells were re-suspended in the AA medium with a 10–100 times dilution prior to perfusing them into the sample chamber. It was necessary to use the AA medium inside the sample as the YPD medium interfered with the poly-L-lysine coating.

Perfusion chambers were constructed by connecting a thin coverslip (Menzel no 1.5) to a thick cover slide by two layers of a double-sided scotch tape. The thin coverslip would be facing the objective. The coverslip was thoroughly cleaned in 70% ethanol whereafter a 10 μ L droplet of 10 mg mL⁻¹ poly-L-lysine (Sigma) in phosphate buffer (10 mM K₃PO₄, 0.1 M KCl) was spread out and allowed to dry on the coverslip. The poly-L-lysine firmly glued the cells onto the coverslip. After the cellular suspension was flushed into the perfusion chamber, it was sealed with vacuum grease to prevent evaporation.

3.2. Equipment

Optical tweezers were formed by implementing an Nd:YVO₄ laser (5W, Spectra Physics BL-106C, 1064 nm) into an inverted microscope (Leica DMIRBE) and focusing it to a diffraction-limited spot using an oil immersion objective (Leica HCX PL APO 100 \times , NA = 1.4, OIL CS). The sample was moved by a piezo-electric translation stage with capacitive feedback (Physik Instrumente P-517.3CL). A quadrant photodiode (QPD) (S5981, Hamamatsu), positioned in the back focal plane of the condenser, provided high-resolution positional information about the granule. The data were acquired by an NI PCI-6040E data acquisition card, which allowed us to read out the positions of the piezo-stage simultaneously with

the voltage signal from the QPD. As earlier described [32], there is a small time delay between the readings of the various channels on the acquisition card, cf point (e) in the overview of the calibration procedure given below. This delay could cause systematic errors and should be taken into account. For the NI PCI-6040E card, we found the delay time to be $(467 \pm 65) \mu$ s.

The granule was also imaged by a CCD camera (All KODAK Pike, 60 Hz) mounted on the side port of the microscope. The Pike camera read out the image in two channels, one in each side of the total frame. An inherent slight voltage difference between the channels made it difficult to conduct measurements across the border between the two sides, hence, no analyzed granule moved across this border. A fixed lens in front of the CCD camera improved the pixel resolution which became (5.56 ± 0.02) nm/pixel, cf point (d) in the overview of the calibration procedure given below.

The piezo-electric stage could be set to move with a given amplitude and at a given frequency. However, we experienced that at high frequencies, the stage was not able to reach the set amplitude. As the exact motion of the stage is important for this work, we quantified the performance of the piezo-stage using a polystyrene bead stuck to the surface. Figure S1 (available from stacks.iop.org/PhysBio/10/046006/mmedia) in the supporting material shows the ratio between the actual amplitude of the stage movement, A_{rec} , (as measured by the capacitive feedback system) and the set amplitude A_{set} as a function of oscillation frequency. The bead's motion was also measured by video microscopy. It is clear that the piezo-stage does not reach the desired amplitude for frequencies above ~ 5 Hz and the value to be used in the formulas should be A_{rec} and not A_{set} . In order to fully characterize the performance of the piezo-stage, we used averages from three experiments with $A_{\text{set}} = 200$ nm, 500 nm and 1000 nm, respectively, as illustrated by the data points in figure S1.

3.3. Experimental procedure

In all the experiments, a timeseries of the positions visited by a trapped endogenous lipid granule was recorded. Occasionally, a second granule would enter the trap during the calibration procedure. To avoid this ambiguity of the trapped object, images were acquired before, during and after the calibration procedure, and the data sets where the trapped object changed visual appearance during the calibration procedure were discarded.

As described in detail in [32], the calibration procedure consists of the following five steps.

- Passive recording, determination of power spectra.
- Active driving and recording, determination of relaxation spectra.
- Direct positional calibration, determination of unit conversion factor β .
- Pixel size calibration, i.e., the determination of the pixel to actual physical length conversion factor.
- Time delay calibration, i.e., determination of the time delay between the detection systems that record position of stage versus the recording of the particle position supplied by the electronics of the quadrant photo diode.

The calibration of pixel size and time delay was performed as described above. Further details may be found in our earlier paper [32].

Passive measurements, point (a). In the passive measurements, a 3 s timeseries of the position of the granule, $x_P(t)$, was recorded with a sampling rate of 22 kHz. This was repeated 30 times.

Active measurements, point (b). In the active measurements, the piezo-stage was driven sinusoidally with an amplitude of $A_S = 100$ nm, in a frequency range [5 Hz, 75 Hz] with 5 Hz decrements. Recordings of $x_P^{(dr)}(t)$ and $x_S(t)$ were performed for 10 s at a sampling rate of 10 kHz. While choosing the driving amplitude, care should be taken that the active motion takes place within the linear response regime of the QPD. Also, the amplitude should be small enough that linear response theories apply, a threshold which is frequency dependent and visualized in figure 2 of [32].

Positional calibration, point (c). Within a certain interval, the so-called linear region, the voltage output from the QPD is proportional to the distance moved by the trapped object with respect to the trap. The linear regime can be determined simply by moving a stuck bead with constant velocity through the laser focus and determine the regime in which there is a corresponding monotonic linear voltage response in the output from the QPD. In the experiments, it is important to stay within this linear region. If κ and x are measured in units corresponding to the direct measurements of position in the setup, the resulting force, $F = \kappa x$, can be determined without the relatively cumbersome and possibly inaccurate determination of the conversion factor β (see below). To see this, note that in equation (8), the immediate determination of power spectra and particle position amplitude involve position recordings in Volt. This implies that the raw results for $P(\omega_S)$ are given in units of $V^2 s^{-1}$ and similarly that A_P is measured in volt. As a result, the direct determination of κ provides the spring constant in units of $N V^{-1}$. With position measured in volts, spring constant times position is right away given in the natural SI unit for force, N .

However, knowledge of β is essential to retrieve an absolute value of κ and of $G(\omega)$. The unit conversion factor β is defined as the ratio of the distance measured in SI units (meters), x_{SI} , to the distance measured in volts, x_V : $\beta = \frac{x_{SI}}{x_V}$. To determine β , the trapped granule was driven sinusoidally with an amplitude of 200 nm at a frequency of 2 Hz for 10 s. This process was performed twice: once while the laser light was impinging on the QPD and once while the image of the driven granule was recorded by the CCD. This procedure was chosen since for the QPD measurements, the diaphragm of the condenser should be left completely open, whereas in the CCD recordings, the diaphragm should be almost closed, to obtain better contrast in the images. The QPD signal was recorded at 10 kHz and the CCD images at 60 Hz. By comparing the QPD signal amplitude with the positional data acquired from analysis of the CCD images, the absolute value of the positional calibration factor, $|\beta|$ was obtained. Care must be taken when adding the appropriate sign of β according to whether x_V grows or decreases for an increasing x_{SI} .

Using a homemade image-processing particle-tracking program operating in NI LabVIEW as well as a freely

available image-tracking program, Video Spot Tracker⁵, the position of the lipid granule was extracted from the recorded images. Good agreement between the output of those two programs was found. Of course, the value of β should be independent of driving amplitude and should be the same before and after the series of active and passive drivings involved in the calibration procedure. Figure S2 (available from stacks.iop.org/PhysBio/10/046006/mmedia) shows that this was indeed the case; however, it also shows that β is only determined within a relatively large error range. The value for β is found as the ratio between the average amplitudes of two sinusoidal signals: the videotracked trajectory (recorded in pixel and converted to μm) and the QPD signal (recorded in volts). Each signal contains 20 complete cycles, with a sinusoidal fit performed in each cycle. Error bars on β are determined via error propagation, from the standard deviation of the average amplitudes.

4. Results and discussion

4.1. Trap stiffness

One of the characteristics of an optical trap is that the spring constant, κ , is proportional to laser intensity. To check that this is also true for the optical trapping potential inside a living cell characterized by our method, we performed a series of calibration experiments using different laser powers (and different stage-driving frequencies for each laser power) and found κ by using equation (6). Figure 1(B) shows κ versus laser power at the sample, error bars include systematic instrumental errors and statistical errors (SEM), with instrumental errors providing the main contribution, in particular, stemming from uncertainty in β and in the time delay factor, described in point (e) of the calibration procedure, cf also [32]. The full line is a linear regression to the data points. Hence, within errors bars, κ increases linearly with laser power within the probed interval, as expected.

The calibration method allows us to extract a value for κ at any given driving frequency (using equation (6)). Yet, we know that the spring constant of the optical trap, for a given object, at a fixed position and laser intensity, should really be a constant, independent of frequency. The only exception for a constant, frequency-independent value, would be caused by the existence of active processes. Therefore, we performed a series of experiments where one endogenous granule inside the cell was oscillated at different frequencies. The solid squares in figure 2(A) display such a dataset. Within the error bars, the data are consistent with κ being independent of the driving frequency and having an average value of $\kappa = (44.9 \pm 13.5)$ pN μm^{-1} .

The value for κ obtained via equation (6) only contains the force contribution from the optical trap. The cytoskeletal network, within which the granule is embedded, may also contribute to the total spring constant, describing the total elastic force on the granule. Via equation (1), we evaluate the effective total spring constant κ_{eff} as the inverse of the response

⁵ Computer Integrated Systems for Microscopy and Manipulations, University of North Carolina; cismm.cs.unc.edu/downloads.

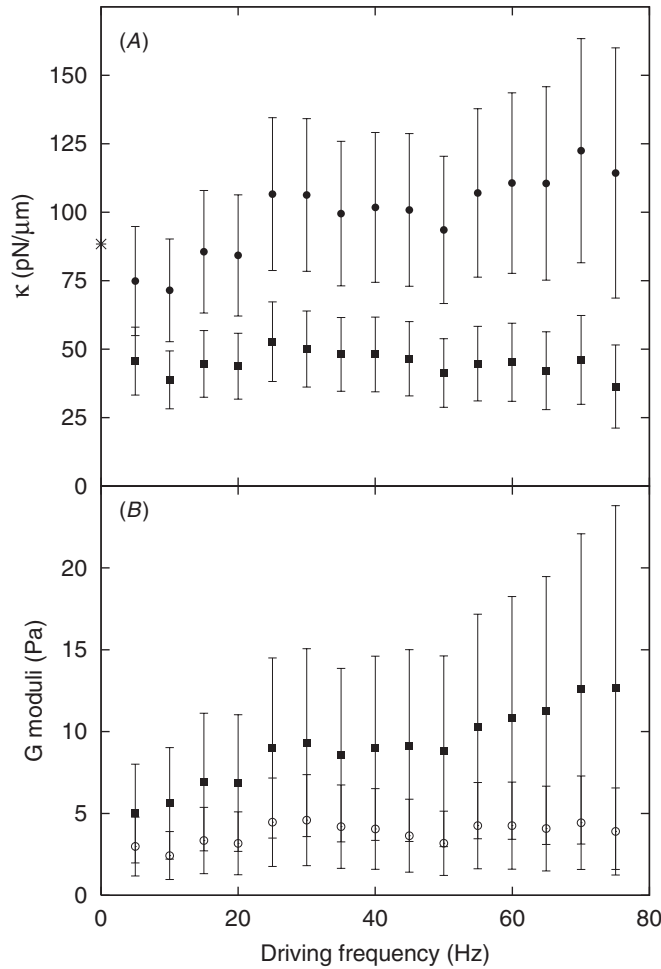


Figure 2. Spring constant and viscoelastic moduli obtained for a single granule inside a living cell driven at different frequencies. (A) Spring constant, κ , characterizing the optical trapping potential inside the living cell as function of driving frequency (solid squares). Error bars represent error propagation of systematic instrumental uncertainties and statistical errors (SEM). Also shown are the values of the effective spring constant, κ_{eff} (solid circles) including the elastic contribution from the cytoplasm. The star indicates the value of $k_B T / \langle x_p^2 \rangle$, indicative of a frequency-averaged effective spring constant, arising from both the optical trap and the elastic contribution of the cytoplasm. (B) Viscoelastic moduli (solid squares denote $\text{Re}[G]$, open circles denote $\text{Im}[G]$) as a function of oscillation frequency. Error bars include systematic instrumental errors (mainly from determination of β and r) and statistical errors (SEM).

function $\chi(\omega)$, cf equations (9) and (10). This effective total spring constant contains both the elasticity of the polymer network in the cytoplasm and the elasticity of the optical trap. Values of κ_{eff} obtained for different driving frequencies are shown in figure 2(A) (full circles). Also, in figure 2(A), the value of $k_B T / \langle x_p^2 \rangle$ is plotted as an asterisk on the ordinate axis. In a viscous system, it would equal the spring constant of the trap. The mechanical drift would tend to increase $\langle x_p^2 \rangle$, and thus one would tend to underestimate the spring constant from such a measurement. In a viscoelastic system, there is no direct correspondence between $k_B T / \langle x_p^2 \rangle$ and the spring constant of the trap [35]. It may, however, be seen as an independent measure for a frequency-averaged effective spring constant, including contributions from both the optical trap and from

elastic elements in the viscoelastic medium. The accordance between $k_B T / \langle x_p^2 \rangle$ and the effective spring constants (solid circles) in figure 2(A) confirms this interpretation.

Active processes inside the cell, for instance mediated by molecular motors, are not accounted for in our derivations. In the experiments presented here, however, within the experimental error bars, we did not encounter variations in the resulting trap spring constant for one granule while changing driving frequency. This is consistent with data in the literature for which active processes are found as a violation of the fluctuation–dissipation theorem [36, 37]; these violations are observed for frequencies below 5 Hz only both in an *in vitro* actin–myosin network system and in MLOY4 cells.

There can be a relatively large variety in κ measured for identical laser intensities among different cells and even at different locations within the same cell. In order to show the strength of the optical trap for different trapped granules, figure 3(A) provides the average values of κ from 22 different granules in 6 different sample preparations. The figure clearly indicates the need for calibrating the trap *in situ* for each individual-trapped object, in particular, if precise force measurements are sought for. The spread in κ might be due to several experimental parameters such as granule size, shape and refractive index (which is related to its contents), together with the refractive index of the surrounding cytoplasmic region. Unlike *in vitro* optical trap experiments with well-characterized artificial beads, here (*in vivo*) we do not control the above-mentioned experimental parameters. These properties can vary from granule to granule, making the trap stiffness different for every experiment, and suggesting that repeated trap calibration is necessary.

Quantitative knowledge of κ within the living cell makes absolute quantitative measurements of forces *in vivo* possible, since $F = \kappa x$. As discussed earlier, the absolute value of F can be found without going through the relatively cumbersome process of quantifying the conversion factor, β . In the data presented here, β values have an average relative error about 18%, cf figure S2, giving rise to a large error in the SI-converted trap stiffness (equation (22) in [32]), and without this large error, a more precise determination of the actual force may be anticipated.

4.2. Viscoelastic moduli

In addition to the characterization of the optical trap *in vivo*, we also extracted values for the viscoelastic moduli of the living fission yeast cells' cytoplasm. These viscoelastic moduli are indicative for cell mechanical properties. The viscoelastic moduli were found using equation (7) and G is shown for one granule as a function of frequency, f , in figure 2(B). The diameters of the trapped granules were needed for the determination of G and were estimated to be $0.6 \pm 0.1 \mu\text{m}$ from bright field microscopy images. The solid squares show $\text{Re}[G]$ (the elastic response) and the open circles $\text{Im}[G]$ (the viscous response), error bars are found from the error propagation of systematic instrumental errors, mainly arising from the determination of β and r , and statistical errors (SEM). $\text{Re}[G]$, also denoted the shear storage modulus or G' , increases

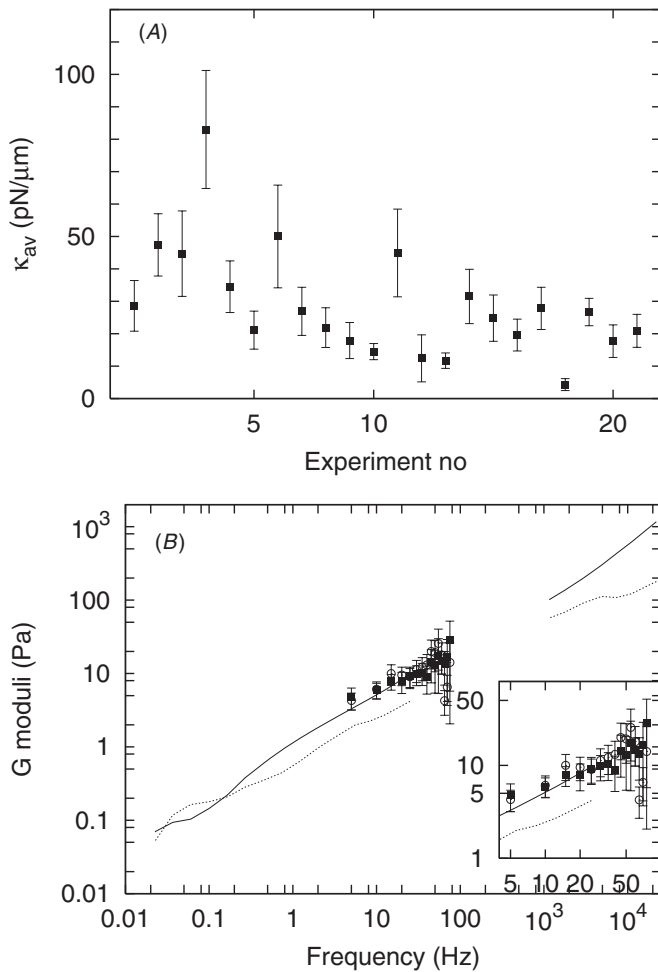


Figure 3. Panel A shows values for the frequency-averaged trap spring constant, κ_{av} , resulting from 22 different granules in 6 different sample preparations, each preparation containing several cells. The relatively large spread in κ from one granule to another probably is due to differences in the trapped granules. Most cells were in interphase, but a few were in the mitotic phase, among those set no 4. Individual error bars are the results of error propagation of instrumental errors and statistical errors represented as standard error on the mean. (B) Average values from all data sets of the viscoelastic moduli as function of frequency. Shear storage moduli, G' , are plotted as solid squares, shear loss moduli, G'' , as open circles. The two lines denote data from [13] which have been re-analyzed to retrieve the corresponding values for G' (full line) and G'' (dotted line). The experiments of [13] were performed with two different methods (video-tracking and laser-tracking) that did not cover the frequency range [100 Hz, 1000 Hz]. The inset zooms in on the frequency range investigated by the experiments reported in this paper.

with f whereas $\text{Im}[G]$, also denoted the shear loss modulus or G'' , in this data set appears independent of driving frequency in the probed interval.

To investigate any scaling properties of G' and G'' versus frequency, the average values obtained for all data sets are plotted on double logarithmic axes in figure 3(B) (G' by the solid squares and G'' by the open circles). Again, we observe an increase of G' with frequency; this increase is well described by an exponent α : $G'(\omega) \propto \omega^\alpha$, where $\alpha = 0.75$. In the same figure, the newly obtained values for G' and G'' are compared

to values given in the literature [13] for the same biological system. In [13], the values of G' and G'' were not given directly, but cast in terms of the mean-squared displacement. However, from this old data set, the corresponding values of G' and G'' were calculated (as described in [38]) and shown in figure 3 as a full line and a dashed line, respectively. Although the majority of our new data fall in the frequency window which was methodologically inaccessible in [13], it is clear that in the frequency interval where the two methods overlap, the absolute correspondence is quite good. In particular, both data sets are well described by a scaling exponent of 0.75, as also found to describe the scaling of G' for an actin network [39, 19]. A slightly smaller value of $\alpha \sim 0.5\text{--}0.6$ was found to describe the scaling properties of G' within the *Dictyostelium* cytoplasm recorded by magnetic microrheology [40].

As our data were taken in a relatively narrow frequency window (limited by acceptable piezo-stage amplitudes), they cluster in an interval from 4 to 30 Pa for the applied frequency window between 5 and 75 Hz. This is one order of magnitude smaller than moduli found by AFM microrheology at the surface of neutrophils [41], and slightly smaller than the instantaneous elastic modulus of entire cells found by micropipette aspiration of human mesenchymal stem cells [42] or of NIH T3 fibroblasts [43]. Our values are slightly larger than the moduli found at 100 Hz in the cytoplasm of HeLa, HepG2 and THLE cells with fluorescence correlation spectroscopy methods [44]. Results of similar magnitude are found using magnetic tracer beads in the cytoplasm of *Dictyostelium* cells and recorded with magnetic microrheology [40]. PC3 human prostatic adenocarcinoma cells explored with a similar method display slightly larger values for cytoplasmic viscoelastic moduli [45] than ours. Viscoelastic moduli have also been obtained by video-tracking of granuli in endothelial cells subject to shear stress, with results for the moduli in a size range (0.1–10 Pa) comparable to our results [46]. Finally, our results compare well with recordings using optical trapping methods on *in vitro* solutions of filamentous actin with the actin-binding protein filament in a concentration ratio 0.04 [19].

5. Conclusion and outlook

We demonstrated how to use a combined active–passive calibration method that allows the determination of force characteristics of an optical trap inside a living organism. This is a necessary step on the way to quantitative force measurements inside living cells using optical traps. As neither the viscoelastic landscape, nor the index of refraction, nor the exact size or shape of the trapped object necessarily are known inside the living cell, it is not trivial to determine the optical trapping strength by normal calibration methods. However, our *in vivo* calibration method works under these boundary conditions. We proved that the hallmarks of optical trapping still prevail inside a living organism, for instance, the data are consistent with the optical trapping strength being proportional to laser power. In comparison to previous work with quantitative force measurements inside cells [47, 22], the calibration of the trap here takes place *in situ*, takes into

account the tracer's local environment and has the option of using the same tracer particle for calibration as for recordings of forces in the live cells.

In addition, the active-passive calibration method allows for the extraction of the absolute value of viscoelastic moduli describing the physical properties of the living cell cytoplasm. We here show results obtained in live fission yeast, *S. pombe*, results that indicate that the local elastic properties of the cytoplasm have significant variations. In future experiments, we suggest rather to move the laser, e.g., by acousto-optic deflectors, than the stage as significantly higher frequencies can then be reached. In future, it will also be interesting to compare the performance of the present procedure to force-determination based on detection of light momentum changes [25, 26], recently also applied in live *Allium cepa* cells [28].

Acknowledgments

We thank G Thon for providing the *S. pombe* cells, IM Tolic-Nørrelykke for the use of data from [13], and H Ma and A Farré for corrections and useful suggestions to the procedure. Some of the error propagation results in the appendix are based on unpublished notes by M Fischer. JM acknowledges an FPU grant from the Spanish Ministry of Education. This work was also financially supported by the University of Copenhagen Excellence Program and by the Technical University of Denmark.

Appendix. Summary of error propagation

Here we summarize the considered error sources for computing error bars on trap stiffness and viscoelastic parameters.

A.1. Error analysis in trap stiffness

A.1.1. Error in active-driving parameters. Active-driving stage and particle signals are fitted to a sinusoidal model in order to determine their amplitude (A_S and A_P , respectively), frequency (ω_s) and phase difference between them ($\Delta\phi_{\text{fit}}$). 95% confidence intervals are obtained for each fitted parameter. NLFIT and NLPARCI functions in MATLAB were used for that purpose. The phase difference is then corrected by the channel delay ($t_{\text{delay}} \pm \Delta t_{\text{delay}}$) associated with signal acquisition:

$$\Delta\phi = \Delta\phi_{\text{fit}} + t_{\text{delay}}\omega_s. \quad (\text{A.1})$$

$$\Delta(\Delta\phi) = \sqrt{(\Delta(\Delta\phi_{\text{fit}}))^2 + (\omega_s \Delta t_{\text{delay}})^2}. \quad (\text{A.2})$$

Note. In practice, the uncertainty on t_{delay} is dominating, and its error contribution is more important at higher frequencies.

A.1.2. Error in β . The β parameter relating voltage to particle position (in SI units) is calibrated as the quotient of amplitudes of video and QPD recordings of the trapped particle trajectory during low-frequency sinusoidal stage driving. The statistical

error arises from the variability of amplitudes (A_{vid} and A_{QPD}) in consecutive sinusoidal cycles for a given organelle. The resulting uncertainty in β is computed as follows:

$$\Delta\beta = \beta \sqrt{\left(\frac{\sigma(A_{\text{vid}})}{\langle A_{\text{vid}} \rangle}\right)^2 + \left(\frac{\sigma(A_{\text{QPD}})}{\langle A_{\text{QPD}} \rangle}\right)^2}. \quad (\text{A.3})$$

A.1.3. Error in power spectrum $P(\omega_s)$. A smooth power spectrum of 3 s passive recordings is obtained by averaging $N = 30$ passive spectra (which had been previously blocked in groups of $n_b = 10$ points). The uncertainty of the power spectral density at a given frequency $P(\omega_s)$ is calculated as follows:

$$\Delta P(\omega_s)/P(\omega_s) = 1/\sqrt{n_b N}. \quad (\text{A.4})$$

A.1.4. Error in temperature. Uncertainty in temperature is estimated to be of 5 K (it is not possible to directly measure the temperature inside the sample).

A.1.5. Error in $\kappa(\omega_s)$. By error propagation using the result of equation (6), one finds

$$\frac{\Delta\kappa(\omega_s)}{\kappa(\omega_s)} = \left[\left(\frac{\Delta T}{T}\right)^2 + \left(\frac{\Delta P(\omega_s)}{P(\omega_s)}\right)^2 + \left(\frac{\Delta A_P(\omega_s)}{A_P(\omega_s)}\right)^2 + \left(\frac{\Delta A_S(\omega_s)}{A_S(\omega_s)}\right)^2 + \left(\frac{\Delta(\Delta\phi)(\omega_s)}{\tan(\Delta\phi(\omega_s))}\right)^2 + \left(\frac{\Delta\beta}{\beta}\right)^2 \right]^{1/2}. \quad (\text{A.5})$$

A.1.6. Error in κ_{av} . The final trap stiffness κ_{av} for a given organelle is calculated as the mean value of the set of n trap stiffnesses at different frequencies $\kappa(\omega_s)$. Error arises from the variability of kappa at different frequencies (SEM) and the individual errors of each measurement:

$$\Delta\kappa_{\text{av}} = \sqrt{\frac{\sigma(\kappa(\omega_s))^2}{n} + \left(\frac{\sum_{\omega_s} \Delta\kappa(\omega_s)}{n}\right)^2}. \quad (\text{A.6})$$

A.2. Error analysis on viscoelastic parameters

A.2.1. Error in G . In order to find the relative error on the values for the viscoelastic modulus, we first resort to a calculation of the error in a quantity $\gamma(\omega)$,

$$\gamma(\omega) \equiv \frac{\tilde{R}(\omega)}{\chi(\omega)}. \quad (\text{A.7})$$

Errors in the value for $\gamma(\omega)$ obtained from the data are calculated from the error propagation of this expression. Only the most dominating relative errors in the real part, $\gamma'(\omega)$, and the imaginary part, $\gamma''(\omega)$ are included:

$$\frac{\Delta\gamma'}{\gamma'} = \sqrt{\left(\frac{\Delta\kappa_{\text{av}}}{\kappa_{\text{av}}} + \frac{\Delta\beta}{\beta}\right)^2 + \left(\frac{\Delta(\Delta\phi)}{\tan(\Delta\phi)}\right)^2} \quad (\text{A.8})$$

$$\frac{\Delta\gamma''}{\gamma''} = \sqrt{\left(\frac{\Delta\kappa_{\text{av}}}{\kappa_{\text{av}}} + \frac{\Delta\beta}{\beta}\right)^2 + \left(2\frac{\Delta(\Delta\phi)}{\tan(\Delta\phi)}\right)^2} \quad (\text{A.9})$$

For the computation of the viscoelastic modulus, $G(\omega)$, cf equation (7), the radius r of each trapped particle was estimated from video images, with Δr uncertainty:

$$\frac{\Delta G'}{G'} = \sqrt{\left(\frac{\Delta \gamma''}{\gamma''}\right)^2 + \left(\frac{\Delta r}{r}\right)^2} \quad (\text{A.10})$$

$$\frac{\Delta G''}{G''} = \sqrt{\left(\frac{\Delta \gamma'}{\gamma'}\right)^2 + \left(\frac{\Delta r}{r}\right)^2} \quad (\text{A.11})$$

Glossary

Schizosaccharomyces pombe. Fission yeast cells (*S. pombe*) are rod-shaped eucaryotic cells. This cell type is often used by biologists in connection with studies of the cell cycle.

Optical tweezers. Optical tweezers is the name commonly used for an optical trap composed of a single-focused Gaussian laser beam. It is a device that allows for manipulation and/or observation of nano- and microscopic particles. Typically, the laser wavelength is chosen in the infrared and laser powers are below 1 W in which case the optical tweezers are almost non-invasive and may safely be used on live biological systems. It is the only ‘nano-tool’ capable of manipulating organelles within the cell without having to disrupt the plasma membrane of the cell. In order to perform quantitative measurements with optical tweezers, the calibration of the trap properties is necessary.

Microrheology. Rheology is the science of investigating materials that show both elastic and fluid behavior, microrheology does so on the microscopic scale. The so-called viscoelastic materials thus investigated are characterized by their frequency-dependent viscoelastic modulus, $G'(\omega) + iG''(\omega)$. The real part, $G'(\omega)$, is also known as the shear storage modulus and is a measure of the elastic energy stored in the system. The imaginary part, $G''(\omega)$, is also known as the shear loss modulus, and $G''(\omega)/\omega$ appears as a frequency-dependent dynamic viscosity when relating stress to strain.

References

- [1] Greenleaf W J, Woodside M T and Block S M 2007 High-resolution single-molecule measurements of biomolecular motion *Annu. Rev. Biophys. Biomol. Struct.* **36** 171–90
- [2] Moffitt J R, Chemla Y R, Smith S B and Bustamante C 2008 Recent advances in optical tweezers *Annu. Rev. Biochem.* **77** 205–28
- [3] Neuman K C and Nagy A 2008 Single-molecule force spectroscopy: optical tweezers, magnetic tweezers and atomic force microscopy *Nature Methods* **5** 491–505
- [4] Veigel C and Schmidt C F 2011 Moving into the cell: single-molecule studies of molecular motors in complex environments *Nature Rev. Mol. Cell Biol.* **12** 163–76
- [5] Dufrene Y F, Evans E, Engel A, Helenius J, Geub H E and Muller D J 2011 Five challenges to bringing single-molecule force spectroscopy into living cells *Nature Methods* **8** 123–7
- [6] Oddershede L 2012 Force probing of individual molecules inside the living cell is now a reality *Nature Chem. Biol.* **8** 879–86
- [7] Gittes F and Schmidt C F 1998 Signals and noise in micromechanical measurements *Methods Cell Biol.* **55** 129–56
- [8] Berg-Sørensen K and Flyvbjerg H 2004 Power spectral analysis for optical tweezers *Rev. Sci. Instrum.* **75** 594–612
- [9] Neuman K C and Block S M 2004 Optical trapping *Rev. Sci. Instrum.* **75** 2787–809
- [10] Rasmussen M B, Oddershede L B and Siegmundfeldt H 2008 Optical tweezers cause physiological damage to *E. coli* and *Listeria* bacteria *Appl. Environ. Microbiol.* **74** 2441–6
- [11] Neuman K C, Chadd E H, Liou G F, Bergman K and Block S M 1999 Characterization of photodamage to *Escherichia coli* in optical traps *Biophys. J.* **98** 2856–63
- [12] Peterman E J G, Gittes F and Schmidt C F 2003 Laser-induced heating in optical traps *Biophys. J.* **84** 1308–16
- [13] Tolić-Nørrelykke I M, Munteanu E L, Thon G, Oddershede L B and Berg-Sørensen K 2004 Anomalous diffusion in living yeast cells *Phys. Rev. Lett.* **93** 078102
- [14] Selhuber-Unkel C, Yde P, Berg-Sørensen K and Oddershede L B 2009 Variety in intracellular diffusion during the cell cycle *Phys. Biol.* **6** 025015
- [15] Jeon J H, Tejedor V, Burov S, Barkai E, Selhuber-Unkel C, Berg-Sørensen K, Oddershede L B and Metzler R 2011 In vivo anomalous diffusion and weak ergodicity breaking of lipid granules *Phys. Rev. Lett.* **106** 048103
- [16] Yamada S, Wirtz D and Kuo S C 2000 Mechanics of living cells measured by laser tracking microrheology *Biophys. J.* **78** 1736–47
- [17] Wei M-T, Zaorski A, Yalcin H C, Wang J, Hallow M, Ghadiali S N, Chiou A and Ou-Yang H D 2008 A comparative study of living cell micromechanical properties by oscillatory optical tweezers *Opt. Express* **16** 8594–603
- [18] Mizuno D, Head D A, MacKintosh F C and Schmidt C F 2008 Active and passive microrheology in equilibrium and nonequilibrium systems *Macromolecules* **41** 7194–202
- [19] Lee H, Ferrer J M, Nakamura F, Lang M J and Kamm R D 2010 Passive and active microrheology for cross-linked F-actin networks *in vitro Acta Biomater.* **6** 1207–18
- [20] Ashkin A, Dziedzic J M, Bjorkholm J E and Chu S 1986 Observation of a single-beam gradient force optical trap for dielectric particles *Opt. Lett.* **11** 288
- [21] Visscher K, Gross S P and Block S M 1996 Construction of multiple-beam optical traps with nanometer-resolution position sensing *IEEE J. Sel. Top. Quantum Electron.* **2** 1066–76
- [22] Sims P A and Xie X S 2009 Probing dynein and kinesin stepping with mechanical manipulation in a living cell *Chem. Phys. Chem.* **10** 1511–6
- [23] Leidel C, Longoria R A, Gutierrez F M and Shubeita G T 2012 Measuring molecular motor forces *in vivo*: implications for tug-of-war models of bidirectional transport *Biophys. J.* **103** 492–500
- [24] Hendricks A G, Holzbauer E L F and Golman Y E 2012 Force measurements on cargoes in living cells reveal collective dynamics of microtubule motors *Proc. Natl Acad. Sci. USA* **109** 18447–52
- [25] Smith S B, Cui Y and Bustamante C 2003 Optical-trap force transducer that operates by direct measurement of light momentum *Methods Enzymol.* **361** 134–62
- [26] Farré A and Montes-Usategui M 2010 A force detection technique for single-beam optical traps based on direct measurement of light momentum changes *Opt. Express* **18** 11955–68
- [27] Farré A, Marsá F and Montes-Usategui M 2012 Optimized back-focal-plane interferometry directly measures forces of optically trapped particles *Opt. Express* **20** 12270–91

- [28] Mas J, Farré A, López-Quesada C, Fernández X, Martín-Bardosa E and Montes-Usategui M 2011 Measuring stall forces *in vivo* with optical tweezers through light momentum changes *Proc. SPIE* **8097** 809726
- [29] Lau A W C, Hoffman B D, Davies A, Crocker J C and Lubensky T C 2003 Microrheology, stress fluctuations, and active behavior of living cells *Phys. Rev. Lett.* **91** 198101
- [30] Tolić-Nørrelykke S F, Schaeffer E, Howard J, Pavone F S, Juelicher F and Flyvbjerg H 2006 Calibration of optical tweezers with positional detection in the back-focal-plane *Rev. Sci. Instrum.* **77** 103101
- [31] Fischer M and Berg-Sørensen K 2007 Calibration of trapping force and response function of optical tweezers in viscoelastic media *J. Opt. A: Pure Appl. Opt.* **9** S239–50
- [32] Fischer M, Richardson A C, Reihani S N S, Oddershede L B and Berg-Sørensen K 2010 Active-passive calibration of optical tweezers in viscoelastic media *Rev. Sci. Instrum.* **81** 015103
- [33] Blehm B H, Schroer T A, Trybus K M, Chemla Y R and Selvin P R 2013 *In vivo* optical trapping indicates kinesin's stall force is reduced by dynein during intracellular transport *Proc. Natl Acad. Sci. USA* **110** 3381–6
- [34] Andersson M, Czerwinski F and Oddershede L B 2011 Optimizing active and passive calibration of optical tweezers *J. Opt.* **13** 044020
- [35] Squires T M and Mason T G 2010 Fluid mechanics of microrheology *Annu. Rev. Fluid Mech.* **42** 413–38
- [36] Mizuno D, Tardin C, Schmidt C F and MacKintosh F C 2007 Nonequilibrium mechanics of active cytoskeletal networks *Science* **315** 370
- [37] Mizuno D, Bacabac R, Tardin C, Head D and Schmidt C F 2009 High-resolution probing of cellular force transmission *Phys. Rev. Lett.* **102** 168102
- [38] Mason T G and Weitz D A 1995 Optical measurements of frequency-dependent linear viscoelastic moduli of complex fluids *Phys. Rev. Lett.* **74** 1250–3
- [39] Palmer A, Mason T G, Xu J, Kuo S C and Wirtz D 1999 Diffusing wave spectroscopy microrheology of actin filament networks *Biophys. J.* **76** 1063–71
- [40] Wilhelm C 2008 Out-of-equilibrium microrheology inside living cells *Phys. Rev. Lett.* **101** 028101
- [41] Lee Y J, Patel D and Park S 2011 Local rheology of human neutrophils investigated using atomic force microscopy *Int. J. Biol. Sci.* **7** 102–11
- [42] Yu H, Tay C Y, Leong W S, Tan S C W, Liao K and Tan L P 2010 Mechanical behavior of human mesenchymal stem cells during adipogenic and osteogenic differentiation *Biochem. Biophys. Res. Commun.* **393** 150–5
- [43] Zhou E H, Quek S T and Lim C T 2010 Power-law rheology analysis of cells undergoing micropipette aspiration *Biomech. Model Mechanobiol.* **9** 563–72
- [44] Guigas G, Kalla C and Weiss M 2007 Probing the nanoscale viscoelasticity of intracellular fluids in living cells *Biophys. J.* **93** 316–23
- [45] Robert D, Nguyen T-H, Gallet F and Wilhelm C 2010 *In vivo* determination of fluctuating forces during endosome trafficking using a combination of active and passive microrheology *PLoS One* **4** e10046
- [46] Dangaria J H and Butler P J 2007 Macrorheology and adaptive microrheology of endothelial cells subject to fluid shear stress *Am. J. Physiol. Cell. Physiol.* **293** C1568–75
- [47] Gross S P 2003 Application of optical traps *in vivo* *Methods Enzymol.* **361** 162